ACCSCIENCE PUBLISHING
An International Journal of Optimization and Control: Theories & Applications
ISSN: 2146-0957 eISSN: 2146-5703
Vol.16, No.2, pp.566-579 (2026)
https://doi.org/10.36922/IJOCTA025480217
IJOCTA
RESEARCH ARTICLE

Coordinated demand-side management and energy storage system for a hybrid photovoltaic–wind microgrid under time-of-use tariffs

Minh-Cuong Nguyen[1,2*]

[1] Education Technology and Adaptive Learning Institute, Thai Nguyen University of Technology, Thai Nguyen, Vietnam
[2] Faculty of Electrical Engineering, Thai Nguyen University of Technology, Thai Nguyen, Vietnam
nmc.etali@tnut.edu.vn

ARTICLE INFO

Article history:
Received: November 29, 2025
1st revised: December 26, 2025
Accepted: December 31, 2025
Published Online: February 3, 2026

Keywords:
Battery energy storage system
Demand-side management
Energy management optimization
Renewable microgrid
Time-of-use pricing

AMS Classification 2010:
90B50; 90C90

ABSTRACT

Widespread electrification and increasing penetration of distributed renewables increase stress on distribution networks and motivate demand-side management (DSM) strategies that coordinate flexible loads and energy storage. This study investigates a grid-connected hybrid microgrid comprising a 5 kW photovoltaic array, a 3 kW wind turbine, a 10 kW h battery energy storage system, and a mixed residential–commercial load of about 54 kW h/day under a three-level time-of-use tariff. An optimization-based energy management framework evaluates three operating strategies: (i) a baseline without DSM or storage, (ii) DSM-only load shifting of 20% of the daily demand from peak to off-peak hours, and (iii) the proposed coordinated DSM + energy storage system schedule that jointly optimizes flexible demand, battery charge–discharge, and grid exchange. Over a 24 h horizon, the coordinated strategy reduces the total daily electricity cost from 3.086 USD to 0.108 USD (96.49% savings), decreases the maximum grid import by 69.25%, eliminates photovoltaic curtailment, and increases the renewable share in load supply from 68.33% to 92.56%, while keeping the battery at an average state of charge of 53.69% with roughly one equivalent complete cycle per day. The magnitude of the cost reduction arises from the selected time-of-use schedule and the assumed day-ahead profiles used in the case study. Battery cycling is reported as an operational indicator rather than as a degradation cost term in the optimization objective. A sensitivity analysis with respect to storage capacity reveals substantial cost reductions up to approximately 10–15 kW h, with diminishing returns beyond this range. The results underscore the value of jointly designing DSM and storage scheduling for cost-effective, renewable-rich microgrids, and provide quantitative guidance for storage sizing under time-varying prices.

1. Introduction

The rapid electrification of end-use sectors, together with the increasing penetration of distributed renewable generation, is placing mounting pressure on distribution networks in terms of congestion, voltage regulation (power quality), and adequacy of flexible resources. In this context, demand-side management (DSM) has become a central pillar of modern power system operation, enabling the reshaping of aggregated load profiles, deferring grid reinforcements, and improving the integration of variable renewable energy sources.[1] Recent reviews confirm that residential DSM schemes now range from simple time-of-use (TOU) based shifting to sophisticated optimization-based programs that coordinate multiple appliances and flexible loads,[1] while microgrid-oriented DSM frameworks emphasize local autonomy and resilience in the presence of distributed generation.[2] In particular, the introduction of several DSM programs, such as peak clipping, valley filling, and load shifting, significantly affects the optimal scheduling and

economic operation of grid-connected microgrids, and thus must be co-designed with generation and storage dispatch.[3]

Alongside the evolution of DSM programs, optimization and control methods have advanced to handle large-scale, multi-criteria decision problems under operational and economic constraints. For large industrial and commercial consumers, recent work on demand-side optimization uses metaheuristics, such as particle swarm optimization and machine learning-inspired predictors, to minimize electricity cost under complex tariffs and operational limits.[4] In parallel, advanced control schemes for dual-storage systems in electric-drive applications account for battery degradation and power split between storage devices, thereby highlighting the importance of jointly optimizing energy flows and asset lifetime.[5] In general, multi-objective regression models and hybrid models enable effective modeling of nonlinear relationships and handle trade-offs among conflicting objectives, such as cost, emissions, and comfort level in energy systems.[6] The same optimization mindset is applied to many other energy-constrained systems, such as coverage path optimization for unmanned aerial vehicles with battery and spatial limitations[7] and to pneumatic systems in hospitals with uncertain demand.[8] Although these systems differ from microgrids, they share standard features: they are hybrid systems subject to inter-temporal constraints, driven by uncertain inputs, and they require a centralized or hierarchical optimization framework to coordinate their subsystems. This shows that DSM and energy management problems in microgrids are fully compatible with the optimization-based approach that modern control and optimization research is moving toward under TOU pricing.

In microgrids, energy storage systems (ESSs) play a key role in peak shaving, load leveling, and enhancing reliability. Studies indicate that ESSs can effectively reduce peak power in islanded microgrids[9]; however, if cycle-induced battery degradation is not taken into account, the resulting operating schedules become inaccurate, and lifecycle costs are underestimated, especially in microgrids with a high share of renewable energy.[10] For residential and community consumption models, the simultaneous integration of demand response (DR), battery charging and discharging, and grid exchange is necessary to properly reflect the interactions among loads, distributed generation, and storage.[11] To cope with this complexity, various multi-stage, stochastic, and probabilistic optimization frameworks have been proposed to address the uncertainty in generation and demand while accounting for risk and battery degradation.[12,13] Advanced scheduling controllers have shown the ability to reduce cost and emissions by optimally coordinating dispatchable resources, ESSs, and DR signals.[14] Research on hybrid photovoltaic–wind–battery microgrids using model predictive control (MPC) or mixed-integer linear programming (MILP) continues to demonstrate that predictive control strategies and detailed modeling improve reliability and economic performance compared with static scheduling,[15] while techno-economic analyses confirm that system performance strongly depends on the relationship between DR, storage capacity, and tariff structures.[16] Recent reviews of DSM and energy management system (EMS) point out that different control architectures (centralized, hierarchical, distributed) lead to distinct trade-offs in flexibility, robustness, and implementation complexity,[17–20] and at the same time stress the growing importance of multi-microgrid operation, cooperation among nodes, and human factors in the optimization process.[21–24]

A decisive aspect in EMS design for microgrids is the accurate modeling of battery degradation. Studies show that if this phenomenon is ignored or oversimplified, short-term optimal results can lead to accelerated aging and higher lifecycle costs.[25–29] Therefore, integrating battery degradation models into the design and operation problem is necessary to determine appropriate ESS sizing and optimal dispatch strategies.[29–34] From an algorithmic perspective, the nonlinearity and discreteness in EMS problems are often handled by hybrid methods that combine metaheuristics and mathematical programming,[34–39] but most existing studies still treat DSM and ESS separately, evaluate only a few isolated indicators, and rarely examine sensitivity to battery capacity or tariff structures.

Recent degradation-aware EMS research has begun to bridge the gap between modeling fidelity and tractability by developing MILP-ready cyclic aging surrogates and multi-year simulations, showing that neglecting degradation can substantially underestimate costs and bias optimal sizing decisions.[25] In parallel, aging-aware control (e.g., MPC-based formulations) indicates that explicitly accounting for calendar and cyclic aging can improve lifetime profitability compared with throughput-based or degradation-blind dispatch.[26,28] For microgrids, data-driven degradation surrogates (e.g., extreme gradient boosting- and neural-network-based predictors) have been embedded into day-ahead scheduling

under uncertainty to co-optimize operational and degradation costs.[27,29] Degradation-aware formulations are also being extended toward joint economic–environmental objectives and tariff-driven operation, with case studies reporting sensitivity to storage sizing/rating choices and market conditions.[30,34] At the system level, recent work increasingly considers flexibility resources and DR alongside storage, using hierarchical or two-layer mixed-integer quadratic programming/MILP frameworks and hybrid intelligent solvers,[31–33,35–38] while recent reviews identify limited multi-criteria evaluation and incomplete DSM–ESS integration as common gaps.[39]

Building on this framework, the present study develops an integrated DSM and ESS scheduling strategy for a grid-connected hybrid photovoltaic (PV)–wind–battery microgrid operating under TOU pricing. The contribution is structured around a transparent comparison of three operating strategies: (i) a baseline case without DSM and without storage, (ii) a DSM-only configuration based on load shifting, and (iii) a coordinated DSM–ESS strategy. System performance is evaluated using a consistent set of quantitative metrics, including daily electricity cost, peak grid import, renewable energy curtailment, renewable energy share, self-consumption ratio, and battery cycling behavior. In addition, a sensitivity analysis of ESS capacity is conducted to explicitly characterize how storage sizing influences operational savings, peak reduction, and renewable utilization, thereby clarifying the trade-offs between investment level and achievable technical and economic benefits. Here, "optimization-based" denotes a deterministic day-ahead scheduling problem posed over a 24-h horizon with hourly resolution. The contribution lies in formulating the DSM load shifting and battery charge–discharge scheduling as a single coupled problem under TOU pricing. The formulation links flexible demand and storage actions through power balance, state-of-charge (SOC) dynamics, and grid-exchange limits at each time step.

2. System modeling

2.1. Hybrid microgrid configuration

The studied system was a grid-connected hybrid PV–wind microgrid with an alternating current (AC) bus, integrating a 5 kW array, a 3 kW wind turbine, a 10 kW h ESS, a single AC load of about 54 kW h/day, and the utility grid under a TOU tariff. Architectures of this type appear widely in recent microgrid energy management studies, where renewable energy source units, storage, and demand-side flexibility interact under dynamic prices.[3,9,14,15] Our configuration, summarized in **Figure 1**, followed this line of work but kept the topology intentionally compact to isolate the effect of DSM and storage coordination.

On the direct current (DC) side, the PV array and wind turbine are interfaced to a common DC bus through appropriate power electronic converters. The PV generator was connected via a unidirectional DC/DC stage with maximum-power-point tracking, while the wind turbine was assumed to be coupled through an AC/DC rectifier followed by a DC link, as in typical small-scale microgrids.[9,15] The ESS was tied to the same DC bus via a bidirectional DC/DC converter that supported both charging and discharging modes and enforced the converter power and current limits.[10,26]

The DC bus fed a single DC/AC inverter, which supplied an AC bus at nominal frequency and voltage. The AC bus connected to a lumped residential/commercial load and to the upstream utility grid. For modeling tractability, the PV array, wind turbine, and ESS were interfaced to the AC bus through a single aggregated DC/AC inverter with a unified power limit. This abstraction was adopted to emphasize energy management interactions at the system level rather than converter-level control and sizing. As a consequence, individual inverter constraints, efficiency curves, and DC-side congestion effects were not explicitly represented in the present model. Similar aggregation models are commonly used in community-scale or campus microgrids.[10,14,21,40] The active power exchange between the AC bus and the grid was denoted as $P_{\text{grid}}(t)$, positive when importing and negative when exporting. The grid was considered an infinite bus with fixed voltage and frequency, but with a time-varying price signal $\lambda(t)$ that reflected TOU tariffs.

The load profile was decomposed into an inflexible part $P_{\text{L,base}}(t)$ (lighting, critical appliances) and a flexible component $P_{\text{L,flex}}(t)$ that could be shifted in time within prescribed bounds. In line with DSM studies that treat 10–30% of the demand as schedulable,[1,2,17,18] we assumed that 20% of the daily energy was flexible. The DSM–ESS controller received measurements and forecasts of PV power $P_{\text{pv}}(t)$, wind power $P_{\text{w}}(t)$, the SOC of the ESS, and the current TOU tariff. Based on these signals, it generated optimal setpoints for the ESS charge/discharge power and for the shifted portion of the flexible load.

Three operating strategies were considered: (i) Strategy A, a baseline case without DSM and without ESS; (ii) Strategy B, in which DSM alone

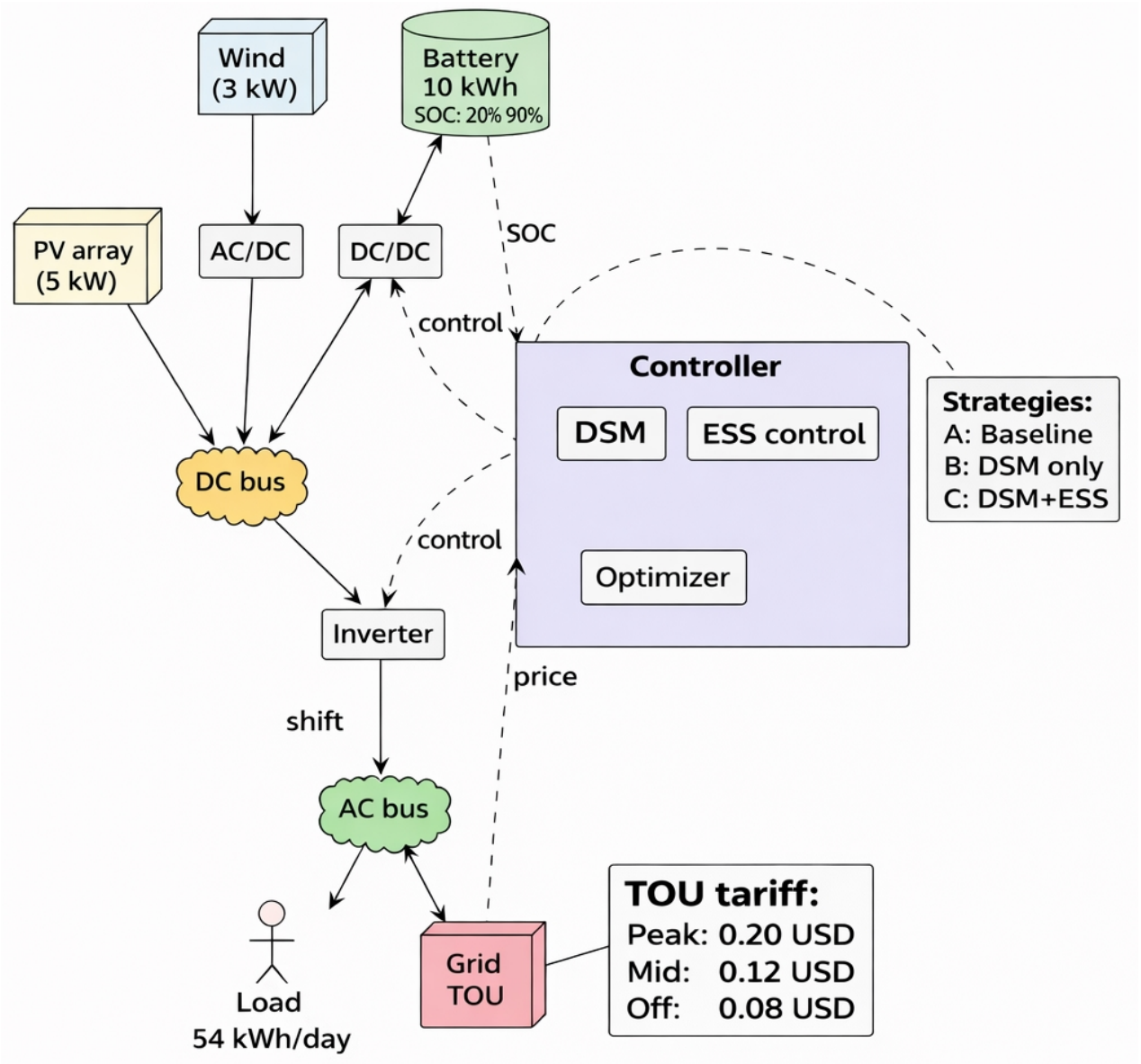

Figure 1. System architecture of the hybrid PV–wind–ESS
Abbreviations: AC: Alternating current; DC: Direct current; DSM: Demand-side management; ESS: Energy storage system; PV: Photovoltaic; SOC: State of charge; TOU: Time-of-use..

shifts part of the flexible load from peak to off-peak periods; and (iii) Strategy C, the proposed coordinated DSM + ESS strategy, where both the load schedule and the ESS operating profile were optimized simultaneously under the TOU tariff.

2.2. Mathematical model

The microgrid was modeled over a discrete-time horizon $t \in 1, \ldots, T$, with a sampling period $\Delta t = 1$ h. All powers are expressed in kW, and all energies in kW h. For compactness, we collected the principal decision variables in the vector $\boldsymbol{u}(t) = (P^{\mathrm{ch}}_{\mathrm{ESS}}(t), P^{\mathrm{dis}}_{\mathrm{ESS}}(t), P^{\mathrm{imp}}_{\mathrm{grid}}(t), P^{\mathrm{exp}}_{\mathrm{grid}}(t), P^{\mathrm{sh}}_{L,\mathrm{flex}}(t))^T$, where $P^{\mathrm{sh}}_{L,\mathrm{flex}}(t)$ denotes the scheduled flexible demand effectively supplied at time (t).

At each time step, active power on the AC bus must balance generation, storage exchange, and demand. Adopting the sign convention used in numerous EMS formulations,[3,10,15,40] we obtained **Equation** (1):

$$\begin{aligned} &P_{\mathrm{pv}}(t)+P_{\mathrm{w}}(t)+P^{\mathrm{imp}}_{\mathrm{grid}}(t)+P^{\mathrm{dis}}_{\mathrm{ESS}}(t) \\ &= P_{\mathrm{L}}(t)+P^{\mathrm{ch}}_{\mathrm{ESS}}(t)+P^{\mathrm{exp}}_{\mathrm{grid}}(t) \end{aligned} \tag{1}$$

where the total load is given by **Equation** (2):

$$P_{\mathrm{L}}(t) = P_{\mathrm{L,base}}(t) + P^{\mathrm{sh}}_{\mathrm{L,flex}}(t) \tag{2}$$

The net grid exchange variable used in the plots is then shown in **Equation** (3):

$$P_{\mathrm{grid}}(t) = P^{\mathrm{imp}}_{\mathrm{grid}}(t) - P^{\mathrm{exp}}_{\mathrm{grid}}(t) \tag{3}$$

To represent curtailed renewable power, we introduced non-negative slack variables, $P_{\text{pv}}^{\text{curt}}(t)$ and $P_{w}^{\text{curt}}(t)$, and enforce the constraint in **Equation** (4):

$$\begin{aligned} P_{\text{pv}}(t) + P_{\text{pv}}^{\text{curt}}(t) &= \hat{P}\text{pv}(t), \\ P\text{w}(t) + P_{\text{w}}^{\text{curt}}(t) &= \hat{P}\text{w}(t) \end{aligned} \tag{4}$$

where $\hat{P}_{\text{pv}}(t)$ and $\hat{P}_{w}(t)$ denote the available PV and wind power profiles from the resource model or measurement. This explicit representation enabled the optimization to account for curtailed energy and to compute indicators such as renewable utilization and self-consumption.[9,26,27]

The ESS $SOC(t) \in [0,1]$ evolves according to the standard discrete-time model used in battery-integrated microgrids[10,11,21,26] as shown in **Equation** (5):

$$\begin{aligned} &SOC(t+1) = SOC(t) \\ &+\frac{\eta_{\text{ch}} P_{\text{ESS}}^{\text{ch}}(t) P_{\text{ESS}}^{\text{dis}}(t)/\eta_{\text{dis}}}{C_r}\Delta t \end{aligned} \tag{5}$$

where C_r is the nominal capacity (10 kW h in this study), and $\eta_{\text{ch}}, \eta_{\text{dis}} \in (0,1]$ denote charge/discharge efficiencies. The corresponding stored energy is $E_{\text{ESS}}(t) = C_r, SOC(t)$.

Operational limits include SOC bounds, as shown in **Equation** (6):

$$SOC_{\min} \le SOC(t) \le SOC_{\max}, \forall t \tag{6}$$

and converter power limits are shown in **Equation** (7):

$$\begin{aligned} 0 \le P_{\text{ESS}}^{\text{ch}}(t) \le P_{\text{ESS}}^{\max}, \\ 0 \le P_{\text{ESS}}^{\text{dis}}(t) \le P_{\text{ESS}}^{\max} \end{aligned} \tag{7}$$

To avoid simultaneous charging and discharging, we used two binary variables $y_{\text{ch}}(t)$ and $y_{\text{dis}}(t)$ using the constraint in **Equation** (8):

$$\begin{aligned} &P_{\text{ESS}}^{\text{ch}}(t) \le y_{\text{ch}}(t) P_{\text{ESS}}^{\max}, \\ &P_{\text{ESS}}^{\text{dis}}(t) \le y_{\text{dis}}(t) P_{\text{ESS}}^{\max}, \\ &y_{\text{ch}}(t) + y_{\text{dis}}(t) \le 1 \end{aligned} \tag{8}$$

which yielded a mixed-integer linear structure similar to previous studies.[12,13,15] In the present case study, the ESS was scheduled hourly, and the optimal solution naturally avoided inefficient charge/discharge overlap due to energy conservation and efficiency losses. Thus, **Equation** (8) can be relaxed without affecting feasibility.

Battery throughput and degradation could be approximated by the total absolute energy processed per day, as shown in **Equation** (9), which defines an energy-throughput indicator to characterize battery utilization under different operating strategies. The metric was not included in the optimization objective and, therefore, did not represent a degradation cost. Its role was limited to post-analysis comparison of cycling intensity across scenarios.

$$E_{\text{cyc}} = \sum_{t=1}^{T} (P_{\text{ESS}}^{\text{ch}}(t) + P_{\text{ESS}}^{\text{dis}}(t))\Delta t \tag{9}$$

We later used **Equation** (9) to compute an equivalent number of complete cycles, as in previous studies.[10,26,27] This indicator did not enter the optimization objective in this paper, but it serves to compare the impact of different strategies on battery usage.

The DSM component reshaped the flexible portion of the demand following the usual paradigm of load shifting under time-varying prices.[1–3,17,18] Let $P_{L,\text{flex}}(t)$ denote the baseline flexible load profile before DSM. The scheduled flexible demand $P_{L,\text{flex}}^{\text{sh}}(t)$ must satisfy an energy conservation constraint, as shown in **Equation** (10):

$$\sum_{t=1}^{T} P_{\text{L,flex}}^{\text{sh}}(t)\Delta t = \sum_{t=1}^{T} P_{\text{L,flex}}(t)\Delta t \tag{10}$$

ensuring that DSM only shifts consumption in time without reducing the total daily energy of the flexible appliances.

Moreover, the total flexible energy was limited to a fraction (alpha) of the daily load, with $\alpha = 0.2$ in this study (**Equation [11]**):

$$\sum_{t=1}^{T} P_{\text{L,flex}}(t)\Delta t = \alpha \sum_{t=1}^{T} P_{\text{L}}^{\text{phys}}(t)\Delta t \tag{11}$$

where $P_{L}^{\text{phys}}(t)$ denotes the physical measured load before DSM. Pointwise bounds enforced that the scheduled flexible demand cannot exceed realistic appliance ratings, as shown in **Equation** (12):

$$0 \le P_{\text{L,flex}}^{\text{sh}}(t) \le P_{\text{L,flex}}^{\max}(t), \nwarrow\!\!\searrow\, \forall t \tag{12}$$

In Strategies B and C, DSM tried to move $P_{L,\text{flex}}^{\text{sh}}(t)$ away from high-price periods while respecting **Equations** (10)–(12). A fully discrete (task-based) formulation could represent each flexible task using start/stop binary variables,[20,24,25] but for this study, the aggregate continuous model remained sufficient to capture the economics of peak-to-off-peak shifting.

Grid import and export powers were constrained by contractual limits, as shown in **Equation** (13):

$$\begin{aligned} 0 \le P_{\text{grid}}^{\text{imp}}(t) \le P_{\text{grid}}^{\text{max,imp}}, \\ 0 \le P_{\text{grid}}^{\text{exp}}(t) \le P_{\text{grid}}^{\text{max,exp}} \end{aligned} \tag{13}$$

allowing us to quantify peak power reduction and to study how DSM and ESS coordination sup-

press high imports during peak TOU periods, in line with the peak-shaving objectives in previous studies.[3,9,16]

The TOU tariff model partitions the day into three price periods, a structure widely adopted in residential and small-commercial tariffs.[1,14,19,29] Let $\mathcal{T}_{\text{off}}, \mathcal{T}_{\text{mid}}, \mathcal{T}_{\text{peak}}$ denote the index sets corresponding to off-peak, mid-peak, and peak hours, respectively. For the considered case, $\mathcal{T}_{\text{off}} = 0, \ldots, 6, 23, \quad \mathcal{T}_{\text{mid}} = 7, \ldots, 16, \quad \mathcal{T}_{\text{peak}} = 17, \ldots, 2.$

The import price $\lambda(t)$ is then defined as **Equation** (14):

$$\lambda(t) = \begin{cases} \lambda_{\text{off}} = 0.08, \ t \in \mathcal{T}_{\text{off}} \\ \lambda_{\text{mid}} = 0.12, \ t \in \mathcal{T}_{\text{mid}} \\ \lambda_{\text{peak}} = 0.20, \ t \in \mathcal{T}_{\text{peak}} \end{cases} \tag{14}$$

in USD/kW h. Exported energy was remunerated at a constant feed-in tariff $\lambda_{\text{feed}}(0.02$ USD/kW h), as is common for small rooftop PV systems.[9,14,40]

For compactness, we converted it to **Equation** (15):

$$\begin{aligned} &\lambda(t) = \lambda_{\text{off}}\chi_{\text{off}}(t) \\ &+\lambda_{\text{mid}}\chi_{\text{mid}}(t) + \lambda_{\text{peak}}\chi_{\text{peak}}(t) \end{aligned} \tag{15}$$

where $\chi(t)$ are indicator functions of the corresponding time sets. This representation helps when embedding the price vector into matrix formulations of the optimization problem.

The study adopted deterministic day-ahead PV, wind, and load profiles with a fixed flexible-energy share to preserve transparency. The formulation represented perfect-foresight scheduling over a 24 h horizon, so Strategy C served as an operational benchmark under the specified TOU tariff. Forecast uncertainty, receding-horizon operation, and degradation-aware cost modeling fell outside the scope of the present study and defined direct extensions of the framework.

3. Proposed optimization strategy

The controller sought an optimal daily schedule for $\boldsymbol{u}(t)$ under three different operating strategies. Each strategy corresponded to a distinct subset of active decision variables and constraints, allowing a clean comparison of the added value of DSM and ESS.

Strategy A represented a conventional grid-connected microgrid without explicit demand management and without storage, similar to numerous baseline cases in the literature.[3,9,14] In this case, the ESS is disabled, as shown in **Equation** (16):

$$P^{\text{ch}}_{\text{ESS}}(t) = 0, P^{\text{dis}}_{\text{ESS}}(t) = 0, SOC(t) = SOC(0), \forall t \tag{16}$$

and the flexible demand follows its original profile, as in **Equation** (17):

$$P^{\text{sh}}_{\text{L,flex}}(t) = P_{\text{L,flex}}(t), \quad \forall t \tag{17}$$

The grid import and export adjusted passively to satisfy **Equations** (1)–(4), resulting in a profile $P^{A}_{\text{grid}}(t)$ driven only by the mismatch between generation and the unmodified load. This scenario established the reference daily cost and peak demand against which Strategies B and C were compared.

In Strategy B, the ESS remained inactive as in **Equation** (17), but the flexible share of demand was scheduled according to **Equations** (10)–(12) to exploit the TOU tariff. The decision variable is $P^{\text{sh}}_{L,\text{flex}}(t)$, while $P^{\text{imp}}_{\text{grid}}(t)$ and $P^{\text{exp}}_{\text{grid}}(t)$ follow from the power balance in **Equation** (1).

To emphasize the 20% flexibility assumption, we define the daily flexible energy (**Equation [18]**):

$$\begin{aligned} &E_{\text{flex}} = \textstyle\sum_{t=1}^{T} P_{\text{L,flex}}(t), \\ &\Delta t = \alpha E_{\text{load}}, \alpha = 0.2 \end{aligned} \tag{18}$$

where E_{load} is the total physical daily energy. Constraints in **Equations** (10)–(12) then ensure that the DSM scheduler reshapes but does not reduce this quantity. The optimal DSM-only schedule thus aims at moving $P^{\text{sh}}_{L,\text{flex}}(t)$ from peak to off-peak and mid-peak hours, following ideas similar to those in previous studies,[1,2,17,18,29] yet adapted here to a single-day deterministic problem under fixed PV and wind profiles.

Strategy C activated both DSM and ESS and constituted the main contribution of this paper. The decision variables now include the full vector $\boldsymbol{u}(t)$, and the optimization jointly schedules: (i) the shifted flexible load, (ii) the charge/discharge power of the ESS, and (iii) the grid import/export power subject to all constraints introduced in **Section 2**. Qualitatively, the controller aims to prioritize the instantaneous consumption of local renewable generation, charge the ESS when surplus PV and wind power are available or when prices are low, and discharge the ESS during peak price periods to reduce imports and mitigate high $P^{\text{imp}}_{\text{grid}}(t)$.

Compared to DSM-only scheduling,[1,3,14] Strategy C leveraged storage to decouple load and generation more strongly, while respecting SOC and converter limits.[10,11,21,26,27] This led to a pronounced peak reduction and high renewable self-consumption in the numerical results.

Mathematically, Strategy C enforced the complete set of constraints in **Equations** (1)–(16) and (18), together with bounds from **Equations** (6)**,** (7)**,** and (10)–(13). The only difference between Strategies B and C lies in the presence of the dynamic SOC constraint in **Equation** (5) and the nonzero ESS powers.

For all strategies, the controller minimized the net daily electricity cost seen from the microgrid perspective. The objective function reads (**Equation [19]**):

$$J = \sum_{t=1}^{T} [P_{\text{grid}}^{\text{imp}}(t), \lambda(t) P_{\text{grid}}^{\text{exp}}(t), \lambda_{\text{feed}}] \Delta t \qquad (19)$$

where $\lambda(t)$ is the TOU import tariff defined in **Equations** (15)–(16) and λ_{feed} is the constant feed-in price. Minimizing (J) under Strategy A yielded the baseline cost J^A; under Strategy B, it gave the best DSM-only schedule; under Strategy C, it provided the optimal coordinated DSM + ESS operation.

4. Results and discussion

This section presents a comprehensive quantitative evaluation of a hybrid PV–wind–ESS system operating under TOU pricing, with particular attention to the effects of DSM and energy storage integration. The results include detailed system parameters, the 24-h energy balance, economic performance indicators, storage-related quantities, and graphical analyses of power flows, SOC evolution, the impact of the tariff, and sensitivity with respect to capacity. These results enable a direct comparison of the three operating strategies, showing that coordinating load shifting with energy storage can reduce dependence on the grid, limit surplus power, and enhance the utilization of renewable energy. In this way, the analysis provides a clear basis for evaluating both the technical and practical economic benefits in the problem of selecting system size and scheduling system operation.

Table 1 describes the configuration of the hybrid PV–wind–ESS microgrid and the time-of-use (TOU) electricity tariff. The selected values represent a small-scale microgrid with 5 kW of PV, 3 kW of wind, and a 10 kW h battery, suitable for a mixed residential–commercial setting. The SOC limits from 20% to 90% reflect realistic operating conditions and balance usable capacity with battery lifetime. The three-level TOU tariff creates a clear economic incentive for load shifting and storage operation.

Table 2 presents the 24-h energy balance of the three strategies. Strategy C eliminated curtailed PV energy with $E_{pv}^{curtailed} = 0$ kW h. Strategies A and B still had 22.77 and 21.35 kW h of surplus energy, respectively. Grid energy imports decreased from 19.84 kW h in Strategy A to 4.66 kW h in Strategy C. The system approached a self-balanced operating state. The charging and discharging energies of the ESS achieved 7.37 and 9.55 kW h, respectively. Surplus renewable energy was effectively utilized.

Table 1. The tariff parameters of the photovoltaic–wind–energy storage system

Parameter	Symbol	Value
Rated PV power	P_{pv}^{rated}	5 kW
Rated wind power	P_{w}^{rated}	3 kW
ESS nominal capacity	C_r	10 kW h
Minimum state of charge	SOC_{min}	0.20
Maximum state of charge	$SOC_{\max}$	0.90
Converter efficiency	η_{conv}	0.97
Maximum ESS power	P_{ESS}^{max}	4 kW
Off-peak tariff	λ_{off}	0.08 USD/kW h
Mid-level tariff	λ_{mid}	0.12 USD/kW h
Peak tariff	λ_{peak}	0.20 USD/kW h
Feed-in tariff	$\lambda_{feed-in}$	0.02 USD/kW h
Time step	Δt	1 h
Simulation horizon	T_{sim}	24 h

Abbreviations: ESS: Energy storage system; PV: Photovoltaic.

Table 3 shows the economic performance under the TOU tariff. The daily electricity cost decreased from 3.086 USD in Strategy A to 0.108 USD in Strategy C. The cost saving was 96.49%. Grid imports during peak hours were significantly reduced. The peak-period cost of Strategy C was 0.502 USD. This value was much lower than the 3.848 USD of Strategy A.

The remarkable reduction in daily cost mainly follows from a shift of net grid import away from the peak-price window and a higher utilization of locally generated renewable energy. Strategy C reduced peak-period purchases from the grid, which drove the largest share of the total bill under the adopted tariff. The reported equivalent cycling level indicated frequent battery utilization under this objective. The present comparison focused on

Table 2. Energy balance under three operating strategies

Energy metric	Strategy		
	A: No DSM, no ESS	**B: DSM only**	**C: DSM + ESS**
E_{pv}^{used} (kWh)	14.23	15.65	15.65
$E_{pv}^{curtailed}$ (kW h)	22.77	21.35	0.00
E_{w}^{used} (kW h)	28.57	32.78	32.78
E_{grid}^{import} (kW h)	19.84	14.21	4.66
E_{grid}^{export} (kW h)	41.30	35.67	28.30
E_{ESS}^{ch} (kW h)	0	0	7.37
E_{ESS}^{dis} (kW h)	0	0	9.55
$E_{unserved}$ (kW h)	0	0	0
E_{pv}^{used} (kW h)	14.23	15.65	15.65

Abbreviations: DSM: Demand-side management; ESS: Energy storage system.

Table 3. Economic performance of each strategy

Economic metric	Strategy		
	A: No DSM, no ESS	**B: DSM only**	**C: DSM + ESS**
Total cost (USD)	3.086	1.495	0.108
Peak-period cost (USD)	3.848	1.760	0.502
Off-peak cost (USD)	0.016	0.401	0.172
Feed-in revenue (USD)	0.826	0.713	0.566
Savings vs. A (%)	0	51.55	96.49

Abbreviations: DSM: Demand-side management; ESS: Energy storage system.

Table 4. Demand-side management and energy storage system performance indicators

Performance metric	Strategy		
	A: No DSM, no ESS	**B: DSM only**	**C: DSM + ESS**
Average SOC (%)	-	-	53.69
Minimum SOC (%)	-	-	20.00
Maximum SOC (%)	-	-	90.00
Eq. complete cycles (cycles/day)	-	-	0.96
Peak reduction (%)	0	46.52	69.25
Self-consumption (%)	50.89	57.59	68.94
Renewable share (%)	68.33	77.32	92.56

Abbreviations: DSM: Demand-side management; ESS: Energy storage system; SOC: State of charge.

short-horizon operational costs, so lifecycle cost impacts from degradation were excluded from economic accounting in this case study. The reported savings quantified the best achievable schedule under the assumed day-ahead inputs; forecast errors in wind and load could reduce the realized benefit in field operation.

Table 4 shows that the average SOC of the DSM + ESS strategy achieved 53.69%. The SOC remained within the 20–90% range. This operating range reflected the optimizer's preference for a short-term reduction in electricity cost under the adopted objective. Without degradation-related costs, this SOC trajectory should not be interpreted as lifecycle-optimal battery operation. The peak power reduction reached 69.25%. The renewable energy share reached 92.56%. Most of the load was supplied from clean sources.

Figure 2 shows the input power of PV, wind, and the total load. PV reached its maximum at midday. Wind generation varied modestly and remained nonzero throughout the day. The load

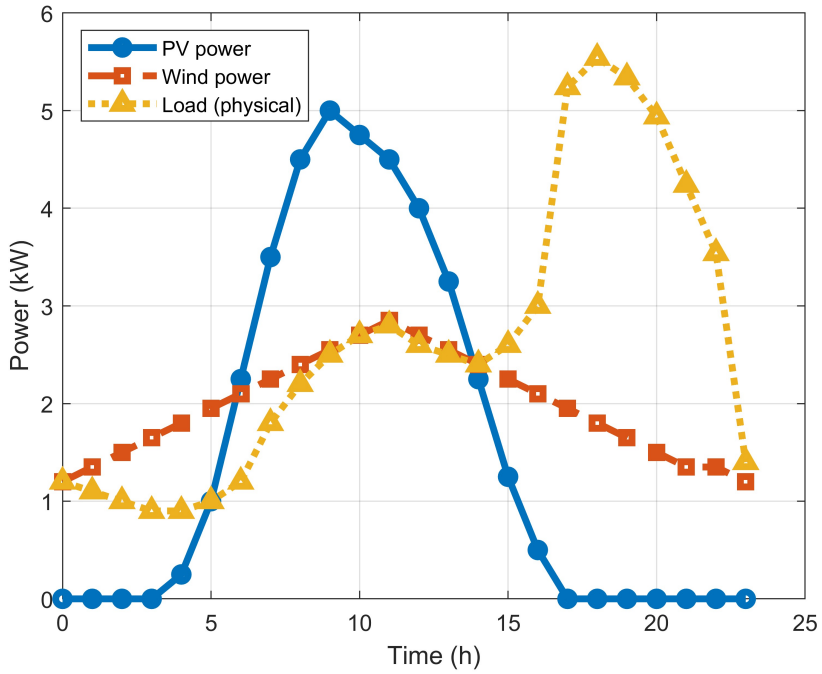

Figure 2. Hourly photovoltaic (PV), wind generation, and load profiles over 24 h.

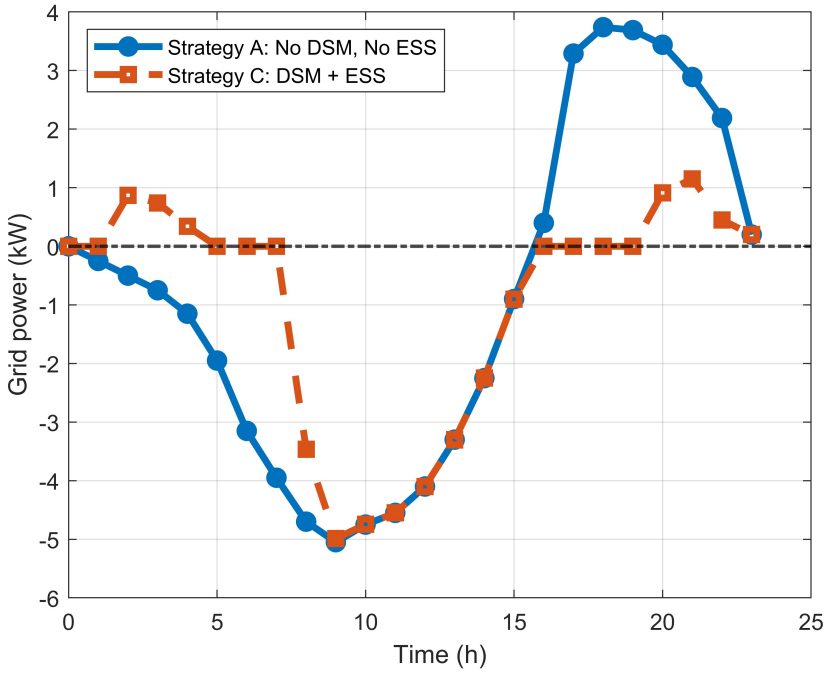

Figure 3. Grid power exchange under Strategy A (no demand-side management [DSM] and energy storage system [ESS]) and Strategy C (with DSM and ESS). Note: Grid power exchange: Import (>0); export (<0).

exhibited two peaks in the morning and evening. The period from about 17:00 to 22:00 was the highest load window. The phase mismatch between generation and consumption necessitates the use of DSM and ESS.

Figure 3 illustrates the grid power exchange in Strategies A and C. The maximum grid import power in Strategy A was approximately 3.85 kW. This value decreased to about 1.18 kW in Strategy C. The reduction was 69.25%. The stress on the grid is clearly reduced.

Figure 4 shows the SOC evolution of the ESS in Strategy C. The SOC was always within the 20%–90% limits. The average value was

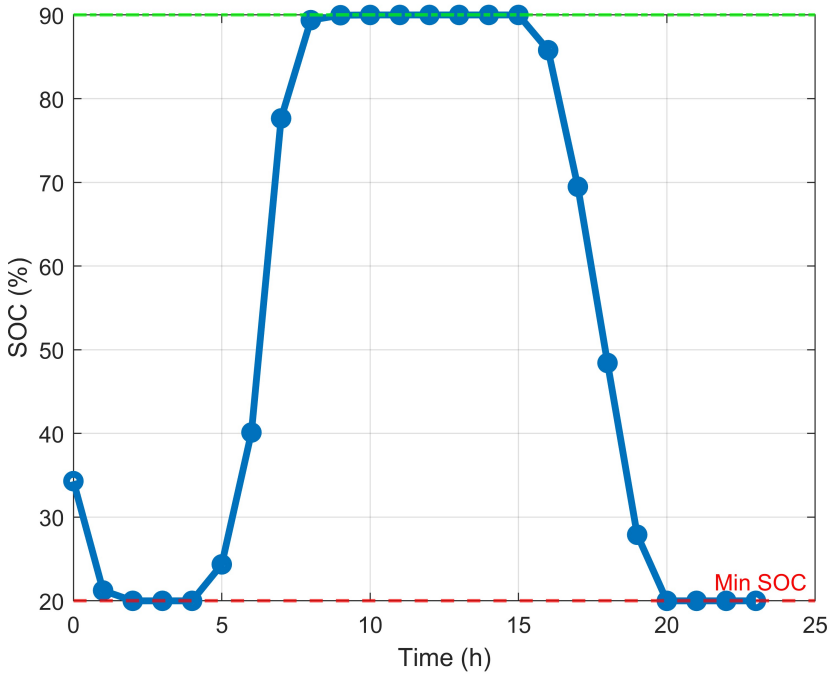

Figure 4. State-of-charge (SOC) trajectory of the energy storage system under Strategy C.

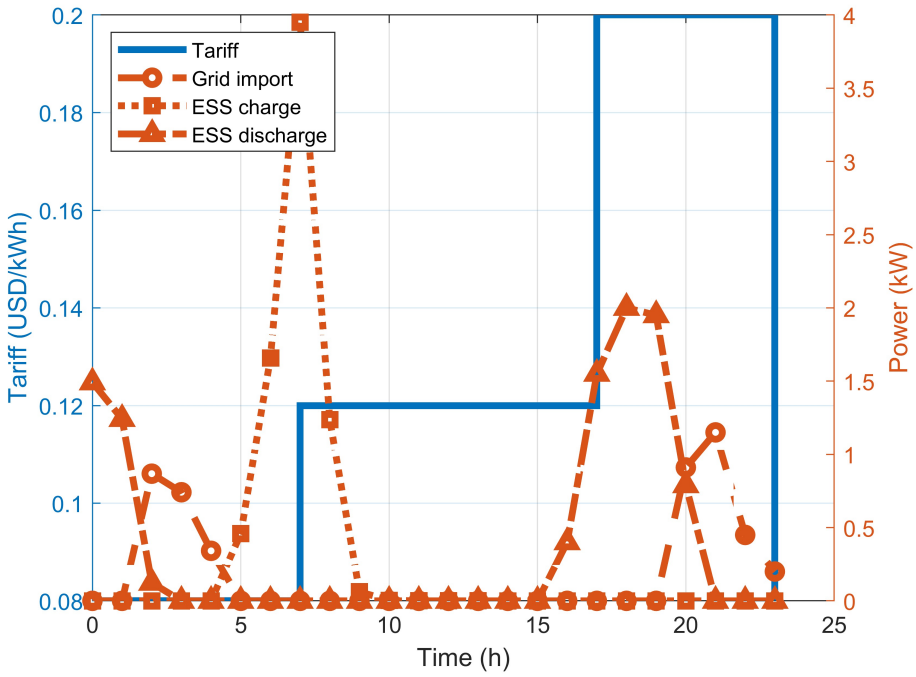

Figure 5. Time-of-use tariff and grid/energy storage system (ESS) charge–discharge.

53.69%. The equivalent number of cycles per day was about 0.96. This level of utilization is considered moderate. Battery lifetime is well preserved.

Figure 5 shows the relationship between the TOU tariff and the charging–discharging behavior of the ESS. The battery was mainly charged during low-price periods and when surplus renewable energy was available. The battery discharged during high-price hours. Grid imports were shifted away from expensive time slots. The total cost is significantly reduced.

Figure 6 compares the cost and renewable energy share of the three strategies. Strategy A had a cost of 3.086 USD and a 68.33% share. Strategy C achieved 0.108 USD and 92.56%. Strategy B

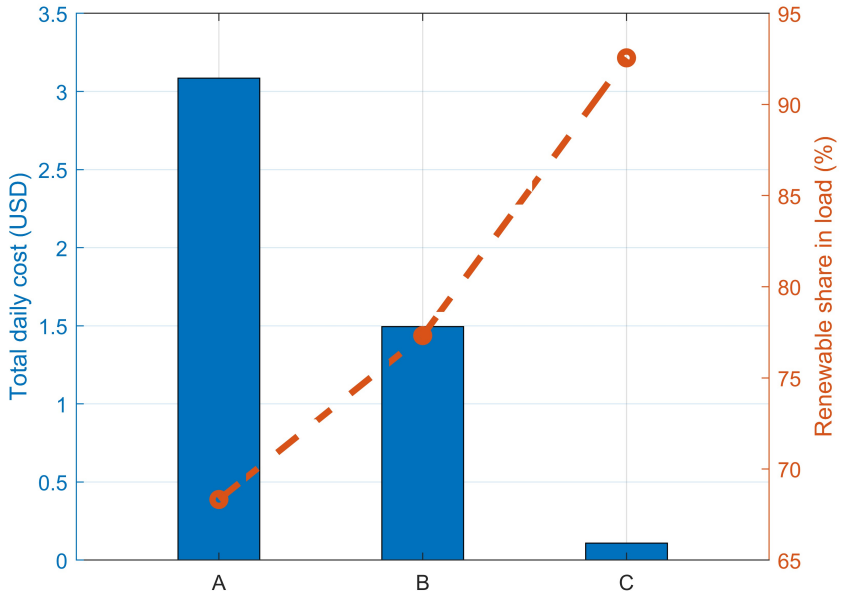

Figure 6. Total daily cost and renewable share comparison for the three strategies.

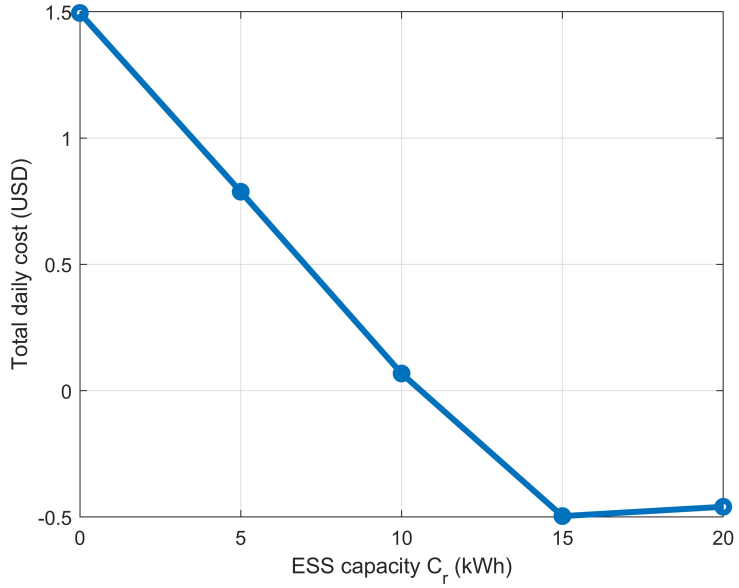

Figure 7. Sensitivity of total daily cost to ESS capacity.

was between the two cases, with a cost of 1.495 USD and a share of 77.32%. The DSM + ESS option delivers the highest performance.

Figure 7 shows the sensitivity of the cost with respect to ESS capacity. The cost decreased rapidly when the capacity increased from 0 to 10 kW h. The rate of reduction slowed down when the capacity exceeded 10–15 kW h. The marginal benefit declined beyond this point. An economically suitable capacity range is identified.

The quantitative values depend on the tariff spread and the alignment between renewable generation and demand in the selected profiles. Different price ratios or profile patterns can change the achievable savings and the preferred storage utilization level. The aggregated interface may overestimate simultaneous utilization of multiple sources compared with a multi-inverter implementation.

5. Conclusion

The study confirms that coordinated DSM and battery scheduling can markedly improve the technical and economic performance of a grid-

connected hybrid microgrid. The results indicate a clear shift toward a self-balanced operating regime, with reduced grid dependence, lowered peak demand, and minimal renewable curtailment. The battery operates within the prescribed SOC bounds, while the observed cycling level reflects short-term operational optimization rather than lifecycle-optimal usage.

From a practical perspective, the results show that coordinated control of flexible demand and storage can deliver greater operational benefits than increasing generation capacity alone. An economically meaningful range of battery capacity is identified before diminishing returns emerge. The reported cost reduction should be interpreted as an operational outcome under the adopted day-ahead setting and tariff structure. Incorporating degradation-aware cost terms is expected to revise both the optimal cycling pattern and the net economic benefit.

Several extensions can strengthen the framework. Renewable generation and load profiles are inherently uncertain, and electricity prices may vary in real time. Detailed battery degradation models and user comfort constraints can be integrated. The coordination scheme can be embedded within forecasting-based control, reinforcement learning, or MPC architectures. Experimental validation represents the final step toward deployment. While no new optimization algorithms are introduced, the study demonstrates that careful coordination of existing DSM and storage scheduling mechanisms yields substantial and interpretable benefits. The presented results, therefore, serve as a pragmatic benchmark for coordinated DSM–ESS operation under TOU pricing, motivating future extensions toward higher-fidelity converter modeling and degradation-aware optimization.

Acknowledgments

The author gratefully acknowledges the support of Thai Nguyen University of Technology and the Education Technology and Adaptive Learning Institute, Thai Nguyen University of Technology, Vietnam.

Funding

None.

Conflict of interest

The author declares no conflicts of interest in this work.

Author contributions

This is a single-authored article.

Availability of data

Data are available from the corresponding author upon reasonable request.

AI tools statement

The author confirms that no AI tools were used in the preparation of this manuscript.

References

1. Mo H, Li C, Liu N, Zhao B, Dong H, Liu H. Energy storage systems for carbon neutrality: challenges and opportunities. *Front Eng Manag.* 2025;12(2):305-329. https://www.doi.org/10.1007/s42524-025-4190-3
2. Elalfy DA, Gouda E, Kotb MF, Bureš V, Sedhom BE. Comprehensive review of energy storage systems technologies, objectives, challenges, and future trends. *Energy Strategy Rev.* 2024;54:101482. https://www.doi.org/10.1016/j.esr.2024.101482
3. De Carne G, Maroufi SM, Beiranvand H, et al. The role of energy storage systems for a secure energy supply: a comprehensive review of system needs and technology solutions. *Electr Power Syst Res.* 2024;236:110963. https://www.doi.org/10.1016/j.epsr.2024.110963
4. Domínguez M, Fernández-Cardador A, Fernández-Rodríguez A, et al. Review on the use of energy storage systems in railway applications. *Renew Sustain Energy Rev.* 2024;207:114904. https://www.doi.org/10.1016/j.rser.2024.114904
5. Ahmad S, Shafiullah M, Ahmed CB, Alowaifeer M. A review of microgrid energy management and control strategies. *IEEE Access.* 2023;11:21729-21757. https://www.doi.org/10.1109/ACCESS.2023.3248511
6. Ahmethodžić L, Musić M, Huseinbegović S. Microgrid energy management: classification, review and challenges. *CSEE J Power Energy Syst.* 2023;9(4):1425-1438. https://www.doi.org/10.17775/CSEEJPES.2021.09150
7. Bakare MS, Abdulkarim A, Zeeshan M, et al. A comprehensive overview on demand side energy management towards smart grids: challenges, solutions, and future direction. *Energy Inform.* 2023;6:4. https://www.doi.org/10.1186/s42162-023-00262-7
8. Panda S, Mohanty S, Rout PK, et al. A comprehensive review on demand side management and

market design for renewable energy support and integration. *Energy Rep.* 2023;10:2228-2250. https://www.doi.org/10.1016/j.egyr.2023.09.049
9. Dahiru AT, Daud D, Tan CW, et al. A comprehensive review of demand side management in distributed grids based on real estate perspectives. *Environ Sci Pollut Res Int.* 2023;30:81984-82013. https://www.doi.org/10.1007/s11356-023-25146-x
10. Ragui K, Bennacer R, Chen L. Pore-scale modeling on supercritical CO_2 invasion in 3D micromodel with randomly arranged spherical cross-sections. *Energy Rep.* 2021;7:33-42. https://www.doi.org/10.1016/j.egyr.2021.05.061
11. Bakare MS, Abdulkarim A, Shuaibu AN, et al. Energy management controllers: strategies, coordination, and applications. *Energy Inform.* 2024;7:57. https://www.doi.org/10.1186/s42162-024-00357-9
12. Yoon Y, Kim H. Charge scheduling of an energy storage system under time-of-use pricing and a demand charge. *Sci World J.* 2014;2014:937329. https://www.doi.org/10.1155/2014/937329
13. Diouf A, Noro Y. Optimal BESS scheduling with real-time assessment for time-of-use customers using particle swarm optimization. In: *Proc 15th Int Conf Power Energy Electr Eng (CPEEE).* Fukuoka, Japan: IEEE; 2025:375-381. https://www.doi.org/10.1109/CPEEE64598.2025.10987270
14. Liu C, Abdulkareem SS, Rezvani A, et al. Stochastic scheduling of a renewable-based microgrid in the presence of electric vehicles using modified harmony search algorithm with control policies. *Sustain Cities Soc.* 2020;59:102183. https://www.doi.org/10.1016/j.scs.2020.102183
15. Ferruzzi G, Graditi G, Rossi F, et al. Optimal operation of a residential microgrid: the role of demand side management. *Intell Ind Syst.* 2015;1:61-82. https://www.doi.org/10.1007/s40903-015-0012-y
16. Kong X, Bai L, Hu Q, et al. Day-ahead optimal scheduling method for grid-connected microgrid based on energy storage control strategy. *J Mod Power Syst Clean Energy.* 2016;4:648-658. https://www.doi.org/10.1007/s40565-016-0245-0
17. Niknami A, Tolou Askari M, Amir Ahmadi M, Babaei Nik M, Samiei Moghaddam M. Resilient day-ahead microgrid energy management with uncertain demand, EVs, storage, and renewables. *Cleaner Eng Technol.* 2024;20:100763. https://www.doi.org/10.1016/j.clet.2024.100763
18. Poddaeva O, Churin P. Numerical simulation of the pedestrian comfort of the microdistrict. *Energy Rep.* 2022;8:1491-1500. https://www.doi.org/10.1016/j.egyr.2022.09.002
19. Dey B, Misra S, Garcia Marquez FP. Microgrid system energy management with demand response program for clean and economical operation. *Appl Energy.* 2023;334:120717. https://www.doi.org/10.1016/j.apenergy.2023.120717
20. Ali S, Besheer AH, Alqunun K, Alshammari AS. Optimal micro-grid battery scheduling within a smart pricing scheme. *Sci Rep.* 2025;15:2690. https://www.doi.org/10.1038/s41598-025-02690-9
21. Wang Q, Li X, Zhang R, Qi Z. Optimal scheduling of microgrid with variable current for energy storage. In: *Proc 40th Chin Control Conf (CCC).* Shanghai, China: IEEE; 2021:1768-1773. https://www.doi.org/10.23919/CCC52363.2021.9549479
22. Keskin K, Urazel B. Fuzzy control of dual storage system of an electric drive vehicle considering battery degradation. *Int J Optim Control Theor Appl.* 2020;11(1):30-40. https://www.doi.org/10.11121/ijocta.01.2021.00848
23. Akca H, Aktas A. Examination and experimental comparison of DC/DC buck converter topologies used in wireless electric vehicle charging applications. *Int J Optim Control Theor Appl.* 2024;14(2):81-89. https://www.doi.org/10.11121/ijocta.1503
24. Mpaka A, Krishnamurthy S. Optimized demand-side management for large power consumers using PSO and MLIP algorithms: a case study of the Western Cape municipality. *Int J Optim Control Theor Appl.* 2025; 025310136. https://www.doi.org/10.36922/IJOCTA025310136
25. Seger PV, Rigo-Mariani R, Thivel P, Riu D. A storage degradation model of Li-ion batteries to integrate ageing effects in the optimal management and design of an isolated microgrid. *Appl Energy.* 2023;333:120584. https://www.doi.org/10.1016/j.apenergy.2022.120584
26. Collath N, Cornejo M, Engwerth V, Hesse H, Jossen A. Increasing the lifetime profitability of battery energy storage systems through aging-aware operation. *Appl Energy.* 2023;348:121531. https://www.doi.org/10.1016/j.apenergy.2023.121531
27. Safavi V, Vaniar AM, Bazmohammadi N, et al. A battery degradation-aware energy management system for agricultural microgrids. *J Energy Storage.* 2025;108:115059. https://www.doi.org/10.1016/j.est.2024.115059
28. Lee J, Kim Y. Novel battery degradation cost formulation for optimal scheduling of battery energy storage systems. *Int J Electr Power Energy Syst.* 2022;137:107795. https://www.doi.org/10.1016/j.ijepes.2021.107795

29. Zhao C, Li X. Microgrid optimal energy scheduling considering neural network based battery degradation. *IEEE Trans Power Syst.* 2024;39(1):1594-1606. https://www.doi.org/10.1109/TPWRS.2023.3239113
30. Keske C, Srinivasan A, Sansavini G, Gabrielli P. Optimal economic and environmental arbitrage of grid-scale batteries with a degradation-aware model. *Energy Convers Manag X.* 2024;22:100554. https://www.doi.org/10.1016/j.ecmx.2024.100554
31. Dougier N, Garambois P, Gomand J, Roucoules L. Multi-objective non-weighted optimization to explore new efficient design of electrical microgrids. *Appl Energy.* 2021;304:117758. https://www.doi.org/10.1016/j.apenergy.2021.117758
32. Essayeh C, Morstyn T. Optimal sizing for microgrids integrating distributed flexibility with the Perth West smart city as a case study. *Appl Energy.* 2023;336:120846. https://www.doi.org/10.1016/j.apenergy.2023.120846
33. Gbadega PA, Sun Y, Akindeji KT. Integrating demand response technique with effective control algorithm for energy management system in a renewable energy based micro-grid. In: *Proc 32nd South Afr Univ Power Eng Conf (SAUPEC).* Stellenbosch, South Africa: IEEE; 2024:1-6. https://www.doi.org/10.1109/SAUPEC60914.2024.10445027
34. Li R, Tu Q, Feng H, Zou Z. Demand response based battery energy storage systems design and operation optimization. *Energy Build.* 2025;338:115738. https://www.doi.org/10.1016/j.enbuild.2025.115738
35. Pramila V, Kannadasan R, Bharathsingh J, *et al.* Smart grid management: integrating hybrid intelligent algorithms for microgrid energy optimization. *Energy Rep.* 2024;12:2997-3019. https://www.doi.org/10.1016/j.egyr.2024.08.053
36. Elias YB, Yousef MY, Mohamed A, et al. Energy management and demand side managementframework for nano-grid under various utility strategies and consumer's preference. *Sci Rep.* 2024;14:25757. https://www.doi.org/10.1038/s41598-024-74509-y
37. Kassab FA, Celik B, Locment F, et al. Optimal sizing and energy management of a microgrid: a joint MILP approach for minimization of energy cost and carbon emission. *Renew Energy.* 2024;224:120186. https://www.doi.org/10.1016/j.renene.2024.120186
38. Moazzen F, Hossain M. A two-layer strategy for sustainable energy management of microgrid clusters with embedded energy storage system and demand-side flexibility provision. *Appl Energy.* 2024;377:124659. https://www.doi.org/10.1016/j.apenergy.2024.124659
39. Kanakadhurga D, Prabaharan N. Demand side management in microgrid: a critical review of key issues and recent trends. *Renew Sustain Energy Rev.* 2022;156:111915. https://www.doi.org/10.1016/j.rser.2021.111915
40. Tran VT, Le CQ, Dinh TV, Nguyen HH, Le VD. Advanced frequency control strategy for power systems with high renewable energy penetration: a battery energy storage system approach. *Int J Optim Control Theor Appl.* 2025;15(4):625-648. https://www.doi.org/10.36922/IJOCTA025150076

Minh-Cuong Nguyen *received his Ph.D. degree in Electrical Engineering from the Graduate University of Science and Technology, Vietnam Academy of Science and Technology (VAST), in 2021. He is currently a lecturer in the Department of Electric Power Systems, Thai Nguyen University of Technology (TNUT), Vietnam, and serves as the Director of the Education Technology and Adaptive Learning Institute at TNUT. His research interests include optimization of energy systems, distributed generation, and distribution systems in deregulated electricity markets. He also focuses on optimal and nonlinear control, renewable energy integration, and the application of intelligent techniques in distributed power grid control.*

https://orcid.org/0009-0000-7543-8937